Transp Porous Med (2007) 68:219–236
DOI 10.1007/s11242-006-9041-z

ORIGINAL PAPER

Water flow between soil aggregates

A. Carminati · A. Kaestner · O. Ippisch · A. Koliji · P. Lehmann · R. Hassanein · P. Vontobel · E. Lehmann · L. Laloui · L. Vulliet · H. Flühler

Received: 20 July 2006 / Accepted: 25 July 2006 / Published online: 29 September 2006

Abstract Aggregated soils are structured systems susceptible to non-uniform flow. The hydraulic properties depend on the aggregate fabric and the way the aggregates are assembled. We examined the hydraulic behavior of an aggregate packing. We focused on conditions when water mostly flows through the aggregates, leaving the inter-aggregate pore space air-filled. The aggregates were packed in 3 mm thick slabs forming a quasi two-dimensional bedding. The larger aggregates were wetted with water and embedded in smaller aggregates equilibrated at a lower water content. The water exchange between wet and drier aggregates was monitored by neutron radiography. The three-dimensional arrangement of the aggregates was reconstructed by neutron tomography. The water flow turned out to be controlled by the contacts between aggregates, bottle-necks that slow down the flow. The bottle-neck effect is due to the narrow flow cross section of the contacts. The water exchange was simulated by considering the contact area between aggregates as the key parameter. In order to match the observed water flow, the contact area must be reduced by one to two orders of magnitude relative to that obtained from image analysis. The narrowness of the contacts is due to air-filled voids within the contacts.

A. Carminati (✉) · A. Kaestner · H. Flühler
Institute for Terrestrial Ecosystems, ETH, Zürich, Switzerland
e-mail: andrea.carminati@env.ethz.ch

O. Ippisch
Interdisciplinary Center for Scientific Computing, University of Heidelberg, Mannheim, Germany

A. Koliji · L. Laloui · L. Vulliet
Soil Mechanics Laboratory, EPFL, Lausanne, Switzerland

P. Lehmann
Laboratory of Soil and Environmental Physics, EPFL, Lausanne, Switzerland

R. Hassanein · P. Vontobel · E. Lehmann
Spallation Neutron Source Division ASQ, Paul Scherrer Institute, Villigen, Switzerland

Keywords Soil aggregates · Water exchange · Neutron radiography · Contact area

1 Introduction

Aggregation affects the movement of water, air and solutes in soils as well as their mechanical stability. Primary particles are aggregated as micro-porous structural units having diameters ranging from less than one millimeter to some centimeters. The pores in-between these structural units may be filled with looser materials or remain empty, depending on the history of the structure formation. Aggregation is common for instance in the plough layer of tilled soils, in biologically active forest soils, and in humus-rich calcareous top soils.

Aggregated soils have a complex three-dimensional geometry that highly affects the hydraulic behavior. The large inter-aggregate pores form the primary pathways for rapid infiltration, causing small-scale preferential flow and accelerating the leaching of solutes (Jarvis 2002). Under prevalent conditions, the inter-aggregate pores are drained and the water redistributes slowly through the micro-pore region of the aggregates. The large difference between the properties of the macro- and micro-porous regions leads to non-equilibrium flow conditions.

Barenblatt et al. (1960) introduced a dual-porosity model to describe the water flow in a medium that exhibits large pores in-between a less permeable matrix. In this model, the porous medium is considered as two superimposed and interacting domains, representing the macro- and micro-porous regions. This concept was implemented in several codes. A recent review can be found in Šimůnek et al. (2003). The hydraulic properties to be used in such dual-porosity models depend on the complex three-dimensional geometry of the aggregates as well as on the properties of the individual aggregates themselves.

In the studies quoted below, various properties of individual aggregates have been investigated. McKenzie and Dexter (1996) developed a method to measure the saturated conductivity of single aggregates. Zimmerman and Bodvarsson (1990) studied the water infiltration into porous blocks of different shape and size. Thoma et al. (1992) investigated the effect of coating on the water transfer between fractures and porous matrix. Gerke and Köhne (2002) investigated the apparently less permeable aggregate coating. Park and Smucker (2005) found that the surface of the aggregates exhibits a larger porosity than the interior. There is still some debate about coating being a general characteristic of aggregated soils or just specific for some soils.

The transition from the scale of individual aggregates to the larger scale of dual-porosity models remains to be conceptualized. In particular, the properties of the micro-porous region of the aggregates have so far received little attention, despite the fact that under prevalent conditions the water flows through the aggregates and the large pores are drained. In this research, we study the water flow trough an aggregate packing, with particular attention to the water exchange between aggregates, aiming at understanding the relevant properties that control the water exchange.

2 Model concepts and approach

When the large pores are drained, the water flows from aggregate to aggregate. The bridging contacts are mostly narrow compared to the aggregate diameter. Therefore,

they act as bottle-necks for the flow and limit the water exchange between aggregates. The hydraulic properties of the contacts depend on the extent and degree of consolidation. In the case of unconsolidated aggregate packings the contacts are almost point-like. Plastic deformation by compaction and cycles of wetting and draining flatten the contacts and increase the contact area (Or and Ghezzehei 2002). According to the existing models (Or 1996), the contacts have been approximated as continuous regions having the same properties as the aggregates. The hydraulic properties of the contacts have not been identified and parameterized so far.

We postulate that the key factor in the water exchange is the area of the contacts: the larger the contacts, the larger is the flow cross section and the faster is the water exchange. We represent neighboring aggregates as homogeneous media linked with a narrow contact area A_{cont} (Fig. 1). Note, the symbols used are given in Table 1. Both the contacts and the aggregate interior are assumed to have the same hydraulic properties, referred to with the subscript agg. The contact area A_{cont} describes the flow impedance of the contacts, including the hypothetically different hydraulic properties of the aggregate skin. It is the effective flow cross section between aggregates.

The water flow in the aggregate region is modeled with the Richards equation in the mixed form:

$$\frac{\partial\theta(h)}{\partial t} - \nabla\cdot[K(\theta)\nabla h] + \frac{\partial K(\theta)}{\partial z} = 0 \tag{1}$$

where θ [$\mathrm{m^3\,m^{-3}}$] is the volumetric water content, K[$\mathrm{m\,s^{-1}}$] the hydraulic conductivity, h[m] is the matric head and z is the depth. In this notation the water potential is decomposed as $\psi_{\text{w}} = (h - z)\rho_{\text{w}}g$, where ρ_{w} is the density of water and g the gravity. For unsaturated soils, h is negative.

The water retention curve $\theta(h)$ is modeled with a modified van Genuchten curve, with the air entry value being used as additional parameter (Vogel et al. 2001):

$$\Theta = \begin{cases} 1 & \text{if } h > h_{\text{e}} \\ \dfrac{\left[1 + [\alpha h]^n\right]^{-1+1/n}}{\left[1 + [\alpha h_{\text{e}}]^n\right]^{-1+1/n}} & \text{if } h \le h_{\text{e}} \end{cases} \tag{2}$$

where $\Theta \equiv [\theta - \theta^{\text{res}}]/[\theta^{\text{sat}} - \theta^{\text{res}}]$, θ^{sat} is the water content at saturation and θ^{res} the residual water content.

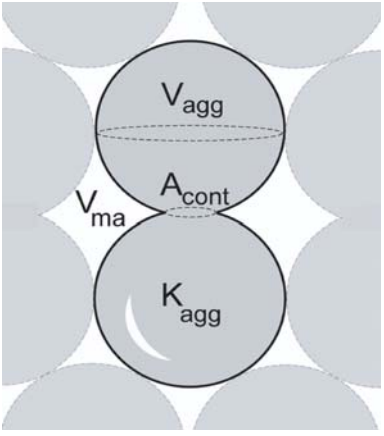

Fig. 1 The water flow through an aggregated medium depends on the properties of the aggregates and on their spatial arrangement. We postulate that the contact area between the aggregates A_{cont} is the key factor for describing the water flow through the aggregates. Neighboring aggregates are described as homogeneous media linked with a narrow contact area A_{cont} (Notation defined in the Table 1)

Table 1 Nomenclature of the symbols used

Symbols	Dimensions	Description
V_{agg}	m^3	Volume of all aggregates
$V_{agg,large}$	m^3	Volume of all large aggregates
$V_{agg,small}$	m^3	Volume of all small aggregates
V_{ma}	m^3	Volume of the inter-aggregate porous space
L_{agg}	m	Aggregate thickness in the beam direction
L_w	m	Water thickness in the beam direction
L_{Al}	m	Thickness of the aluminum walls of the tank
I	neutrons $m^{-2}\,s^{-1}$	Transmitted neutron beam intensity
I_0	neutrons $m^{-2}\,s^{-1}$	Incoming neutron beam intensity
Σ	m^{-1}	Neutron attenuation coefficient
θ	$m^3\,m^{-3}$	Volumetric water content, approximated as $\theta \equiv \frac{L_w}{L_{agg}}$
θ^{sat}	$m^3\,m^{-3}$	Water content at saturation
θ^{res}	$m^3\,m^{-3}$	Residual water content
Θ	$m^3\,m^{-3}$	Water saturation
K	$m\,s^{-1}$	Hydraulic conductivity
K^{sat}	$m\,s^{-1}$	Hydraulic conductivity at saturation
h	m	Matric head, capillary pressure head
α	m^{-1}	van Genuchten parameter, (air-entry value)$^{-1}$
n	–	van Genuchten parameter, pore size index
h_e	m	Air entry value for $\theta(h)$ (Vogel et al., 2001)
τ	–	Tortuosity parameter in the Mualem model
Q	m^3	Volume of water flown from the large to the small aggregates
S_{large}	m^2	Area containing all large aggregates in the 2D field of view
S_{small}	m^2	Area containing all small aggregates in the 2D field of view
d	m	Distance from the boundary between S_{large} and S_{small}
A_{cont}	m^2	Effective contact area between all large and all small aggregates
A_{cont}^{ima}	m^2	A_{cont} estimated by image analysis

The hydraulic conductivity is described using the approach of Mualem (1976):

$$K(\Theta) = K^{sat}\Theta^{\tau}\left[\int_0^{\Theta}\frac{1}{h(\Theta)}d\Theta \Big/ \int_0^{1}\frac{1}{h(\Theta)}d\Theta\right]^2 \tag{3}$$

where K^{sat} is the conductivity at saturation. Ippisch et al. (2006) showed that for fine textured materials the usage of a parameterization with an air entry value, like the modified van Genuchten model given in Eq. 2, is necessary to get physically correct estimations of the hydraulic conductivity curve using the Mualem approach. To model the flow under conditions when the large pores are drained, the Richards equation is solved in the region of the aggregate volume V_{agg}.

In this study, we monitored the water exchange between neighboring aggregates by means of neutron radiography. The three-dimensional geometry of the aggregate packing was obtained by means of neutron tomography. The observed water exchange

was then numerically simulated solving the Richards equation in the three-dimensional aggregate packing. The water exchange was matched by adapting the saturated hydraulic conductivity of the aggregates $K_{\mathrm{agg}}^{\mathrm{sat}}$ and the contact area A_{cont} (Fig. 1). The contact area is adjusted by stepwise removing some contact voxels (Sect. 3.5). Note that A_{cont} is not a parameter to be embedded in Eq. 1, but it is a value that depends on the three-dimensional spatial domanin used for the numerical simulation. The two variables $K_{\mathrm{agg}}^{\mathrm{sat}}$ and A_{cont} can be independently identified, because $K_{\mathrm{agg}}^{\mathrm{sat}}$ controls the water redistribution within the individual aggregates and A_{cont} the exchange across the contacts.

3 Materials and methods

3.1 Neutron radiography and tomography

The water redistribution in the aggregate medium was monitored by means of neutron radiography and tomography. A collimated neutron beam is transmitted through the sample. The measured beam intensity behind the sample carries the information about the mass of the neutron-attenuating materials. Neutron and X-ray techniques complement each other. In particular, neutrons are efficiently attenuated by hydrogen nuclei (Pleinert and Lehmann 1997), making water well detectable relative to other soil components.

The attenuation of the neutron beam intensity through the sample is described with the exponential law:

$$I(x,z) = I_0(x,z)\mathrm{e}^{-\Sigma L(x,z)} \tag{4}$$

where (x,z) is the pixel location, $I_0(x,z)$ and $I(x,z)$ are the incoming and the transmitted beam intensities, $L(x,z)$ is the thickness of the sample, Σ the linear attenuation coefficient. For water $\Sigma_w = 0.347\,\mathrm{mm}^{-1}$, while for dry soil it is approximately $0.06\,\mathrm{mm}^{-1}$. The exponent in Eq. 4 is a composite of the attenuation coefficient of the different materials contained in the sample:

$$\Sigma_{\mathrm{tot}} L_{\mathrm{tot}}(x,z) = \Sigma_1 L_1(x,z) + \Sigma_2 L_2(x,z) + \cdots + \Sigma_n L_n(x,z) \tag{5}$$

The index tot is used for the mixture of the materials $1,2,\ldots,n$. Neutrons are attenuated by absorption and scattering. Eq. 4 is only, valid if the scattered neutrons do not reach the detector. In reality, the radiograms are blurred to a certain extent by scattered neutrons. This leads to an underestimation of the neutron attenuation coefficient. We used a correction algorithm based on Monte Carlo methods to compute the intensity contribution of the scattered neutrons (Hassanein et al. 2005). With such a correction the maximum thickness of water that can be quantified is 1 cm. Beyond this thickness only about 1% of the beam is transmitted unless weakly attenuating materials are used for the liquid phase as for instance heavy water D_2O.

The experiment was performed at the neutron radiography facility NEUTRA, Paul Scherrer Institut (PSI), Switzerland. The beam diameter width can be varied from 15 cm to 40 cm and the flux from 2.5×10^7 to 3.5×10^6 neutrons $\mathrm{cm}^{-2}\,\mathrm{s}^{-1}$. Depending on the sample size and detector system, the exposure time for a single radiograph is about 10 s with a linear spatial resolution of 0.125 mm pixel. For tomography, a set of 301 radiograms is recorded by rotating the sample by 180°. Computed tomography algorithms yield the three-dimensional array of the local neutron attenuation

coefficient. The time required for one tomogram is in the order of 1 h for a sample with a radius of several centimeters and therefore too long to monitor the transient water redistribution in real time. For this reason, we monitored the redistribution as a time series of two-dimensional radiograms and determined the three-dimensional tomogram of the sample after reaching a quasi equilibrium state of the water redistribution. During the last hour, the water exchange was negligible. Note, that the sample thickness in the beam direction is only 3 mm (Sect. 3.3) and the equilibration time is not excessively long, even under unsaturated conditions.

3.2 Materials

Aggregates were collected from a clay loam (Abist, North of Zurich, Switzerland) at a depth of 20–30 cm, E-B horizon (Richard and Lüscher 1983). The same aggregated material was used in the solute transport studies reported by Schulin et al. (1986). Aggregates were separated by sieving and sorted in large (4–8 mm in diameter) and small aggregates (2–4 mm). We packed these aggregates in a mini-tank of inner side lengths of $50 \times 50 \times 3$ mm to obtain a quasi two-dimensional array of large aggregates embedded in small aggregates (Sect. 3.3). The mini-tank was made entirely of aluminum, a material with a low neutron attenuation coefficient. To fit the large aggregates into the mini-tank, they were shaped with sandpaper to disc-like slices of 3 mm thickness. This technique is less prone to disturb the aggregate fabric as cutting them with a scalpel.

The water retention curve was obtained with a pressure plate apparatus. A horizontal layer of aggregates was put onto the porous plate. A negative pressure head was applied by stepwise increasing the air pressure in the closed chamber while the outlet underneath the pressure membrane was kept at atmospheric pressure. We applied a matric head from $h = -0.2$ m to $h = -10$ m. After equilibration, aggregates were weighed, dried at 105°C, and weighed again. The gravimetric water content θ_{grav} was calculated. The water retained represents both, that inside the aggregates and also the menisci in the niches adjacent to the contacts between aggregates. The volumetric water content θ is related to the gravimetric water content θ_{grav} according to

$$\theta = \theta_{\mathrm{grav}} \frac{[1 - \phi_{\mathrm{agg}}]\rho_{\mathrm{solid}}}{\rho_{\mathrm{w}}} \tag{6}$$

where $\rho_w = 0.998\,\mathrm{Mg\,m^{-3}}$ is the density of water and $\rho_{\mathrm{solid}} = 2.6\,\mathrm{Mg\,m^{-3}}$ is the density of the solids. The aggregate porosity, ϕ_{agg}, was measured by Hg-porosimetry, obtaining $\phi_{\mathrm{agg}} = 0.45 \pm 0.10\,\mathrm{m^3\,m^{-3}}$. The experimentally determined water content at saturation was, however, only $\theta^{\mathrm{sat}} = 0.39\,\mathrm{m^3\,m^{-3}}$ as shown in Fig. 2.

Additional information characterizing individual aggregates was obtained by synchrotron tomography performed at the Swiss Light Source (SLS) (Lehmann et al. 2005). Dry aggregates of size 3–5 mm were scanned with a linear voxel size of 1.75 μm. At this resolution, the pores larger than approximately 5 μm are discernible. By means of a pore network model, Kaestner et al. (2005) calculated the air entry value to be $h_{\mathrm{e}} = -0.5$ m. We fitted the water retention data with the modified van Genuchten curve (Eq. 2). The obtained parameter set is shown in Table 2.

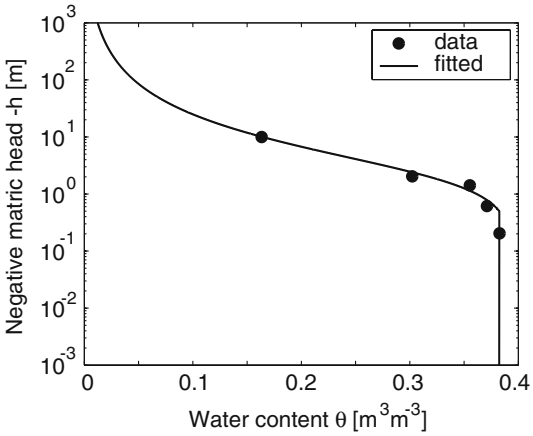

Fig. 2 Water retention curve of the aggregates $\theta(h)$. The data (dots) are determined by stepwise drainage of an aggregate assembly. The data are fitted with a modified van Genuchten curve (Eq. 2). The parameters are reported in Table 2

Table 2 Parameter set of the modified van Genuchten model determined by stepwise draining an aggregate assembly

α[m^{-1}]	n[–]	θ^{sat}[-]	θ^{res}[-]	τ[-]	h_{e}[m]
0.44	1.57	0.39	0	0.5	−0.5

3.3 Experimental setup

The initial water content of the aggregates was conditioned in the following way: the 3 mm thick slices of the large aggregates were saturated on a porous plate by capillary rise and afterwards equilibrated at a matric head $h = -0.2$ m. The small aggregates were put in a small chamber next to a reservoir of water. They were left enclosed for three weeks to equilibrate at a relative humidity close to saturation. The two sets of aggregates were separately stored in air-tight containers. Just before being exposed to the neutron beam, the large aggregates were randomly placed in the mini-tank and the space between them was filled with the small aggregates (Fig. 3).

The moment of embedding was the start of the water exchange between large and small aggregates. Then, the chamber was closed and exposed in the neutron beam for radiography. Every 30 s a picture was taken (Fig. 4). After 1 h, the time step was increased to 5 min. The time-series of neutron radiograms yields the water redistribution in two dimensions. Since the thickness of the mini-tank is roughly the same as the diameter of the small aggregates and the thickness of the prepared large aggregate slices, there was nearly no overlap of the aggregates in the beam direction and the flow from the large to the small aggregates was predominantly perpendicular to the neutron beam. From $t = 4$–5 h no more water content change was detectable. At $t = 5$ h, the sample was tomographed in a state of quasi equilibrium. The tomogram yielded the three-dimensional geometry of the aggregate assembly. Subsequently, the chamber was opened and left at ambient air humidity for 2 months. The tomogram of the air-dried state was used as reference image.

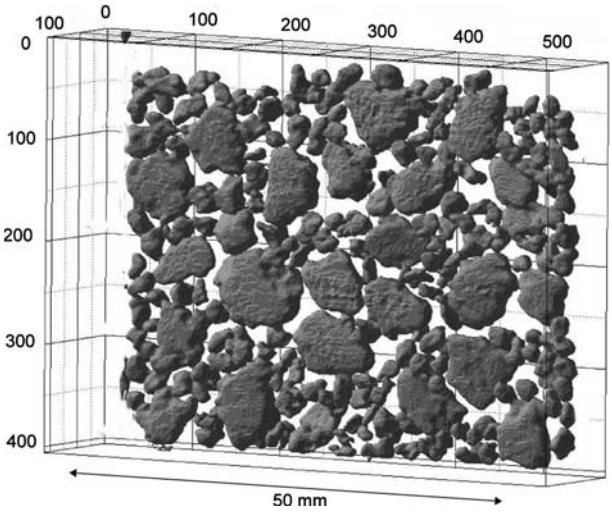

Fig. 3 The three-dimensional spatial distribution of the aggregates in the mini-tank of inner side lengths $50 \times 50 \times 3$ mm. The distribution of the aggregates is reconstructed by neutron tomography at a resolution of 0.125 mm voxel size. The axis are labeled with grid numbers

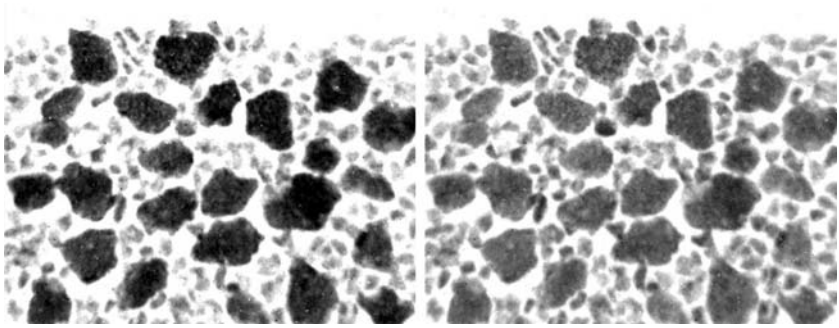

Fig. 4 Neutron radiogram of the aggregate packing at $t \approx 0$ (left) and at $t = 280$ min (right). The gray values represent the mass of the neutron-attenuating materials—i.e. primarily of the water. At $t \approx 0$ the large aggregates are wetter and darker than the small ones. After $t = 280$ min the water redistributed between the aggregates

3.4 Quantification of the water content

The radiograms are gray scale images with the dimensions of 1024×1024 pixels and pixel width of 0.125 mm. According to Eq. 4, the attenuation of the beam in the location (x, z) at time t is:

$$I(x,z,t) = I_0(x,z)\mathrm{e}^{-[\Sigma_{\mathrm{Al}}L_{\mathrm{Al}}(x,z)+\Sigma_{\mathrm{w}}L_{\mathrm{w}}(x,z,t)+\Sigma_{\mathrm{solid}}[1-\phi_{\mathrm{agg}}]L_{\mathrm{agg}}(x,z)]} \tag{7}$$

with $\Sigma_{\mathrm{w}} = 0.347\,\mathrm{mm}^{-1}$ and $\Sigma_{\mathrm{Al}} = 0.0098\,\mathrm{mm}^{-1}$, where the subscript Al refers to the aluminum of the mini-tank walls. The Σ_{solid} depends on the material composition of the soil, L_{agg} is the aggregate thickness in the beam direction, and L_{w} the thickness of water.

The initial settling of the aggregates in the vertically positioned chamber left a small empty space at the top. This region was used to calculate the attenuation of the aluminum walls of the chamber: $\Sigma_{\mathrm{Al}} L_{\mathrm{Al}}(x,z)$.

Neutron tomography yields the three-dimensional arrangement of the aggregates. The gray value data obtained by tomography were segmented in large and small aggregates and in inter-aggregate pore space. The segmentation was done with a double threshold method (Soille 2003): the lower threshold was identified according to Otsu (1979), while the second threshold was set equal to the maximum of the second mode of the histogram. The tomogram was cut-out to a smaller region including the aggregate packing. It has a grid of $436 \times 561 \times 112$ with a grid spacing of 0.125 mm. The binary image of the sample is shown in Fig. 3. From the binary image we calculated L_{agg} and the total volume occupied by all the aggregates, $V_{\mathrm{agg}} = 4.62 \times 10^3\,\mathrm{mm}^3$.

Due to minor shrinking the tomogram of the air-dry sample could not be directly compared to that observed during the water-redistribution, but contained information about the attenuation of the solid phase. From the total attenuation of the dry sample we calculated $\Sigma_{\mathrm{solid}}[1-\phi_{\mathrm{agg}}] = 0.051\,\mathrm{mm}^{-1}$.

Assuming a uniform aggregate porosity and material composition and hence a uniform $\Sigma_{\mathrm{solid}}[1-\phi_{\mathrm{agg}}]$, we obtain from Eq. 7:

$$L_{\mathrm{w}}(x,z,t) = -\frac{\ln\left(\frac{I(x,z,t)}{I_0(x,z)}\right) + \Sigma_{\mathrm{Al}} L_{\mathrm{Al}}(x,z) + \Sigma_{\mathrm{solid}}[1-\phi_{\mathrm{agg}}] L_{\mathrm{agg}}(x,z)}{\Sigma_{\mathrm{w}}} \tag{8}$$

and

$$\theta \equiv \frac{L_{\mathrm{w}}(x,z,t)}{L_{\mathrm{agg}}(x,z)} \tag{9}$$

A gray value threshold for L_{agg} was chosen in order to avoid too small values of L_{agg} and hence division by zero. A median-filter was used to remove the noise error in $I(x,y,t)$. Combining Eqs. 8 and 9 defines the water content distribution over time in the two-dimensional field of view. Integrating $L_{\mathrm{w}}(x,y,t)$ over the tank-area yields the amount of water contained in the sample $V_{\mathrm{w}} = 722 \pm 2.6\,\mathrm{mm}^3$. The standard deviation is obtained by integrating $L_{\mathrm{w}}(x,y,t)$ at the various time steps. The estimation of the amount of water by image analysis is in good agreement with the value $V_{\mathrm{w}} = 800\,\mathrm{mm}^3$, measured by weighing the sample before and after air-drying. The error of 10% can be an expression of neutron scattering and error propagation in the gravimetric water content determination. Therefore, in this analysis we use mainly the difference in water content relative to its initial value $\Delta\theta(x,z,t) \equiv \theta(x,z,t) - \theta(x,z,t=0)$ rather than its absolute value.

3.5 Identification of the three-dimensional geometry of the aggregate packing

The water exchange between large and small aggregates depends on their spatial arrangement. In particular, the contacts play a dominant role. The geometry of the contacts is obtained from the tomogram. By means of a watershed algorithm (Vincent and Soille 1991) we labeled each individual aggregate. The aggregates were classified in large and small aggregates according to their volumes. A close-up of the three-dimensional segmentation is shown in Fig. 5 center.

By averaging L_{w} in the region occupied by all large and all small aggregates, respectively, we obtained the initial water content of 0.21 for the large aggregates and of

Fig. 5 Vertical section of the aggregate packing (close-up). Left: tomogram. The aggregate surface appears fuzzy. The estimation of the contact area by image analysis is uncertain. Center: the tomogram after being segmented in large aggregates (black), small aggregates (gray) and macro-pores (white). Right: the contacts have been eroded for matching the water exchange between the large and small aggregates (pointed out in circles)

0.05 for the small ones which correspond to a degree of saturation of 0.54 and 0.13, respectively. From the identification of large and small aggregates, we calculated the imaged contact area between all large and the surrounding small aggregates $A_{\text{cont}}^{\text{ima}}$. By counting the number of boundary voxels between large and small aggregates and multiplying this value with the side area of a voxel ($0.125 \times 0.125\,\text{mm}^2$), we obtained $A_{\text{cont}}^{\text{ima}} = 231.3\,\text{mm}^2$.

The estimation of A_{cont} by image analysis is inexact because the aggregate edges appear blurred, with a smooth transition from soil to voids over approximately 3–4 voxels (Fig. 5 left). Fissures and pores situated within the contact regions cannot be detected if such openings are smaller than the voxels. The image analysis therefore overestimates the contact area. For a better understanding of the properties and size of the contact area, we determine A_{cont} by simulating the water exchange between aggregates in three-dimensionional experimental packing. The contact area is varied by stepwise removing some contact voxels. To this end we: (1) identified the large and the small aggregates, (2) selected the voxels at the boundary between large and small aggregates, and (3) eroded this set of boundary voxels. With this procedure only the contact voxels are modified, whereas the volume of the aggregates was not significantly altered (Fig. 5). We refer to the two estimates as $A_{\text{cont}}^{\text{ima}}$ from image analysis and A_{cont} from flow simulation.

3.6 Observed water flow

The initial conditions applied to our soil sample are: high water content in the large aggregates and low water content in the small ones. In order to quantify the water exchange between them, we distinguish the areas of the two ensemble of all large and all small aggregates, named S_{large} and S_{small}, respectively. The areas S_{large} and S_{small} are obtained by identifying the regions loosing and receiving water, respectively. This operation was done by dividing the initial radiogram by the final one and selecting the regions of negative and positive $\Delta\theta$s. This analysis is two-dimensional. The spatial pattern of S_{large} and S_{small} is shown in Fig. 6.

We define $Q(t)$ as the cumulative volume of water that moves from S_{large} to S_{small} since the beginning of the experiment. Using Eq. 7 we calculated $Q(t)$ as:

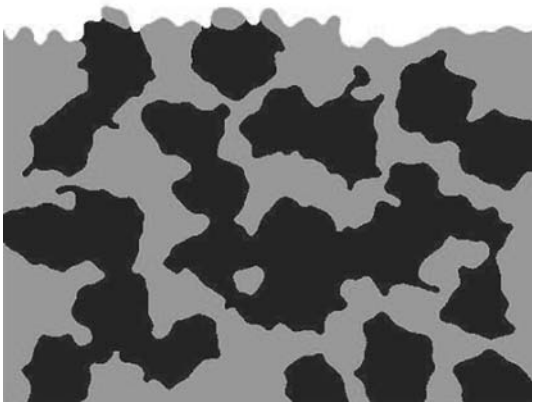

Fig. 6 Regions corresponding to all the large aggregates (S_{large}, black) and all the small ones (S_{small}, gray) in the two-dimensional field of view of the radiogram

$$Q(t) = -\int_{S_{\text{large}}} \Delta L_w(x,z,t)\mathrm{d}s = \frac{1}{\Sigma_{\text{w}}}\int_{S_{\text{large}}} \ln\left(\frac{I(x,z,t)}{I(x,z,t=0)}\right)\mathrm{d}s \tag{10}$$

where ds is the infinitesimal area element located in (x,z). The plot $Q(\sqrt{t})$ is linear (Fig. 7), which is in accordance with the theories of infiltration into homogeneous porous media (Philip 1957).

The cumulative water exchange $Q(t)$ is not sufficient to describe the flow field. It does not contain any information on the distribution of the water within the aggregates, i.e. no information on the change along the linear transects through neighboring aggregates. It is comparable with an outflow experiment without information on the soil moisture status in the transport region.

To describe how water is distributed in the two-dimensional plane, we define d as the distance from the boundary that separates S_{large} and S_{small} (Fig. 8). As a convention, we set d negative within S_{large} and positive within S_{small}. In Fig. 8 we plot the water content, $\theta(d,t)$ and $\Delta\theta(d,t)$ as measured at different times t and calculated according to Eqs. 8 and 9.

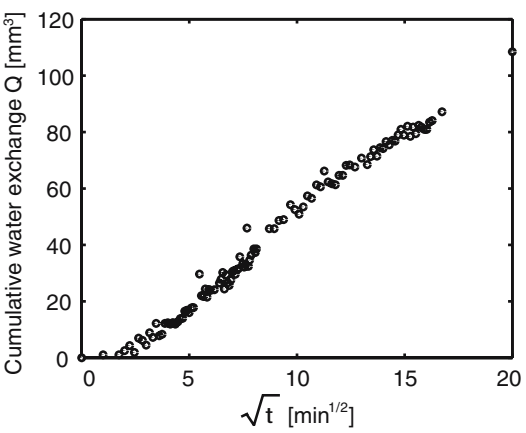

Fig. 7 Cumulative volume of water that moved from large to small aggregates since the beginning of the experiment

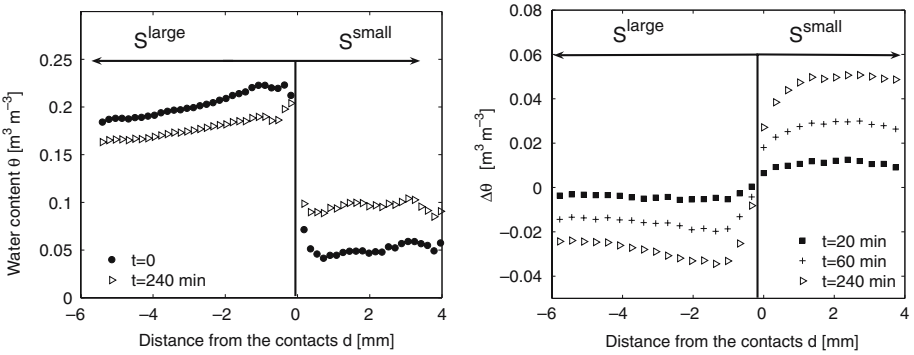

Fig. 8 Water distribution between large and small aggregates: $\theta(d, t)$ at the initial and final time (left) and its difference relative to the initial state (right). The variable θ inside the aggregates remains fairly uniform but drops abruptly at the contacts. This indicates a strong flow impedance at the contacts

Figure 8 shows that θ remains fairly uniform inside the aggregates and changes abruptly at the contacts. This indicates that the contacts have a strong flow impedance compared to the aggregate interior.

In the following analysis, we focus on the boundary between S_{large} and S_{small}, i.e. only at $d = 0$, that is the primary contact area between the large wet aggregates and the small initially drier ones.

3.7 Flow simulation

We simulated the observed water flow by numerically solving the Richards equation (Eq. 1) in the three-dimensional geometry of the aggregate packing. The geometry of the packing is obtained by segmenting the tomogram in aggregates and macro-pores (Fig. 3). A close-up of the spatial domain is shown in Fig. 9.

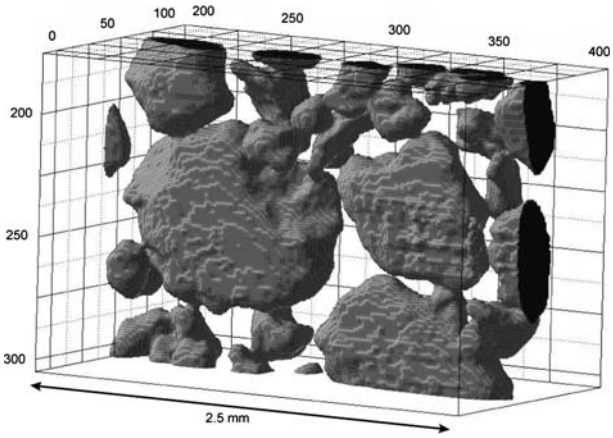

Fig. 9 Close-up of the three-dimensional spatial domain used for the numerical simulation. The entire grid is 436 × 561 × 112 and the voxel size 0.125 mm. The axis are labeled with grid numbers. The geometry is obtained by neutron tomography. The spatial domain is composed of two materials: the aggregates and the macro-pores. In the flow simulation the macro-pores are assumed to be drained, as they were in the experiment

To identify the geometry of the contacts between aggregates by image analysis is rather uncertain. Therefore, the contact area A_{cont} is treated as a variable to be determined by matching the water exchange. The imaged contact area $A_{\text{cont}}^{\text{ima}}$ is used as initial guess. Subsequently, the contact area is adjusted by stepwise eroding the contact voxels until there is an acceptable match between the simulated and observed water exchange.

To solve the Richards equation, we need to define $\theta(h)$ and $K(\theta)$ of aggregates and macro-pores. The functions $\theta(h)$ and $K(\theta)$ are parameterized according to the Van Genuchten model modified by Vogel et al. (2001) (Eq. 2) and the approach of Mualem (Eq. 3). The following set of parameters is required: $\alpha, n, \theta^{\text{sat}}, \theta^{\text{res}}, h_{\text{e}}$ for $\theta(h)$, and τ and $K_{\text{agg}}^{\text{sat}}$ for $K(\theta)$. The parameters for the water retention curve of the aggregates $\theta_{\text{agg}}(h)$ have been independently measured (Table 2). The parameter τ is set to 0.5 as often found in the literature (Mualem 1976). The saturated conductivity $K_{\text{agg}}^{\text{sat}}$ is optimized by matching the modeled and observed water flow. For the parameters of the macro-porous region, we observe that under the given experimental conditions the macro-pores were drained and no flow occurred in them. Moreover, evaporation from the entire region (mini-tank) was prevented by sealing. To describe these conditions, we set K to zero and h_{e} to a large value, so defining a no flow boundary between aggregates and macro-pores. The set of parameters is reported in Table 3.

As initial conditions we set the water content at time zero equal to that obtained by neutron radiography (Eqs. 8, 9):

$$\theta(x,y,z,t=0) = \begin{cases} 0.21 & \text{if } (x,y,z) \in V_{\text{agg,large}} \\ 0.05 & \text{if } (x,y,z) \in V_{\text{agg,small}} \\ 0 & \text{if } (x,y,z) \in V_{\text{ma}} \end{cases} \tag{11}$$

where $V_{\text{agg,large}}$ and $V_{\text{agg,small}}$ are the regions of the large and small aggregates, respectively, and V_{ma} is the macro-pore region. The boundary conditions are no flow at the boundaries. The functions to be fitted are $Q(t)$, $\theta(d,t)$ and $\Delta\theta(d,t)$. They contain the relevant information on the water exchange and distribution within the aggregates. The spatial domain for the numerical simulation is a $54 \times 70 \times 34$ mm cut-out (subregion) of the segmented tomogram that includes all the aggregates (Fig. 3). It has a grid of $436 \times 561 \times 112$ with a grid spacing of 0.125 mm.

The water flow is simulated using the mixed form of Richards equation Eq. 1. The Richards equation is solved for the primary variable h with a new numerical code, which uses a cell-centered finite-volume scheme, full-upwinding in space, and an implicit Euler scheme in time. The non-linear equations resulting from discretization of Eq. 1 are linearized by an incomplete Newton-method with line-search (Bastian 1999). The linear equations are solved with an algebraic multi-grid solver (Braess 1995). For the time solver, the time step is automatically adapted. The model is optimized for numerical stability even if sharp discontinuities of the hydraulic properties are present. Hence, it is well suited for modeling microscopic redistribution processes

Table 3 Set of parameters for $\theta(h)$ and $K(\theta)$ for the numerical simulation. K^{sat} and A_{cont} indicated with † are the fitting variables

	α	n	θ^{sat}	θ^{res}	h_{e}	τ	K^{sat}	A_{cont}
Aggregates	0.44	1.57	0.39	0	0.5	0.5	†	†
Macro-pores	11	5	0.3	0	0	0.0035	0	

in structured soils. The numerical code was already used successfully in Bayer et al. (2005), Vogel et al. (2006) and Ippisch et al. (2006).

4 Results

The contact area A_{cont} and $K_{\text{agg}}^{\text{sat}}$ are adjusted in order to simulate the observed water flow in three dimensions. The functions to be fitted are $Q(t)$, $\theta(d,t)$ and $\Delta\theta(d,t)$.

As initial guess, we used the geometry obtained by image analysis—i.e. we set $A_{\text{cont}} = A_{\text{cont}}^{\text{ima}} = 231.2\,\text{mm}^2$. Then, we adjusted $K_{\text{agg}}^{\text{sat}}$ in order to match $Q(t)$. We obtained an acceptable match with $K_{\text{agg}}^{\text{sat}} = 8 \times 10^{-9}\,\text{m s}^{-1}$ (Fig. 10a). But, $\theta(d,t)$ exhibits a different behavior: the observed $\theta(d,t)$ remains uniform inside the aggregates with an abrupt change at the contacts. Consequently $\Delta\theta(d,t)$ extends uniformly within the aggregates. Instead, the simulated $\theta(d,t)$ varies mostly close to the contacts and the hydraulic gradients become more similar throughout the intra-aggregate and contact regions (Fig. 10b, c). The reason is that the imaged contacts are too large to describe the flow impedance of the contacts.

The contact area is then reduced to achieve a good match for both, $Q(t)$ and $\theta(d,t)$. To compensate the impeding effect of narrower contacts, $K_{\text{agg}}^{\text{sat}}$ was increased. The parameters $K_{\text{agg}}^{\text{sat}} = 1.0 \times 10^{-7}\,\text{m s}^{-1}$ and $A_{\text{cont}} = 8.3\,\text{mm}^2$ turned out to produce a good match between the observed and simulated curves (Fig. 10d–10f).

In Fig. 11, we plot the profile of h within neighboring aggregates simulated with the above parameters. In the negative range of the x-axis (a large and initially wet aggregate), the hydraulic gradient is very small. The gradient has a peak close to the contacts ($d \approx 0$), and then extends in the region of the small and initially dry aggregates.

The value $K_{\text{agg}}^{\text{sat}} = 1.0 \times 10^{-7}\,\text{m s}^{-1}$ agrees well with data reported by McKenzie and Dexter (1996) and Park and Smucker (2005). The value $A_{\text{cont}} = 8.3\,\text{mm}^2$ corresponds to extremely narrow contacts. It was obtained by reducing the contacts down to only two to three voxels. The area of a single contact turns out to be in the order of the voxel side area of $0.015\,\text{mm}^2$. A plausible reason of such narrow contacts is the presence of chained pores and niches within the contacts (Fig. 12). Such pores are due to the irregularity and roughness of the aggregate surfaces and are likely larger than the pores within the aggregates, the latter being subjected to longer consolidation processes than the former. The large pores within the contacts are getting easily drained under the experimental conditions, Thereby reducing the flow cross section. This hypothesis was verified by high resolution X-ray tomography of dry aggregates (Kaestner et al. 2005). The aggregate skin of such aggregates was not compacted, even at the resolution of a few microns. Instead, we observed the presence of large fissures in the aggregate surfaces, possibly the result of occasional shrinking of the drying surfaces. In the case of unconsolidated soils such as our aggregate packing, irregular surfaces cause sparse and narrow contacts and large pores within them. The drainage of large pores within the contacts is properly described by reducing A_{cont}, with no need to introduce a low permeability skin layer. Including such a skin layer would add new parameters without improving the description of the physical processes.

The sensitivity analysis for the evaluation of A_{cont} is shown in Fig. 13, where we plot $Q(t)$ calculated for different values of A_{cont} keeping the conductivity $K_{\text{agg}}^{\text{sat}} = 1.0 \times 10^{-7}\,\text{m s}^{-1}$ constant. The water exchange turns out to be highly sensitive to A_{cont}:

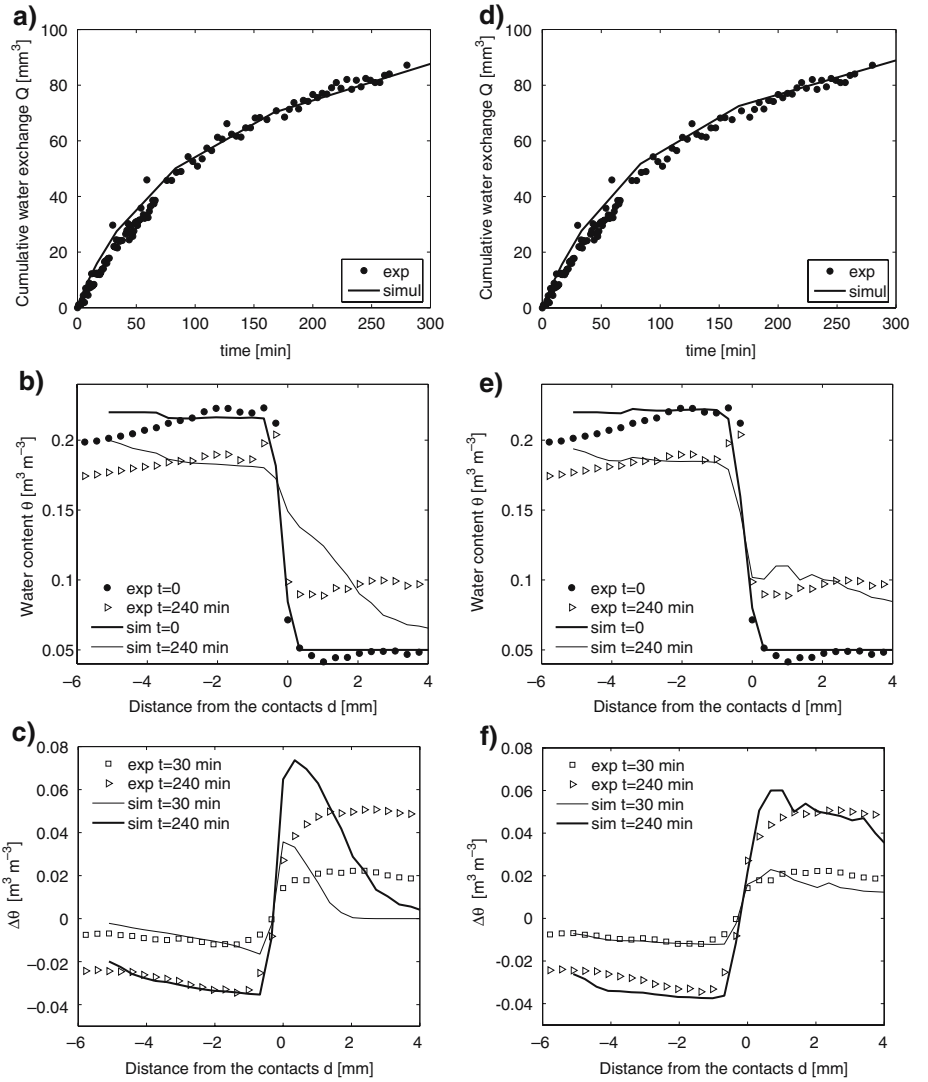

Fig. 10 Observed and simulated water exchange between large and small aggregates. Left (**a**, **b**, **c**): simulation with $A_{\text{cont}}^{\text{ima}} = 231\,\text{mm}^2$ and $K_{\text{agg}}^{\text{sat}} = 8 \times 10^{-9}\,\text{m s}^{-1}$. $Q(t)$ is acceptably matched, but $\theta(d,t)$ exhibits a different behavior: the observed $\theta(d,t)$ remains uniform inside the aggregates with an abrupt change at the contacts, while the simulation exhibits a gradual θ-gradient throughout the domain. Right (**d**, **e**, **f**): simulation with a reduced contact area $A_{\text{cont}} = 8.3\,\text{mm}^2$ and a larger conductivity $K_{\text{cont}}^{\text{sat}} = 1.0 \times 10^{-7}\,\text{m s}^{-1}$. $Q(t)$ and $\theta(d,t)$ are acceptably reproduced. By reducing the contact area we capture the impedance of the contacts

for $A_{\text{cont}} = 8.3\,\text{mm}^2$ we obtain $Q(t = 3\,\text{min}) = 3\,\text{mm}^3$ while for $A_{\text{cont}} = 231.2\,\text{mm}^2$ we get $Q(t = 3\,\text{min}) = 31\,\text{mm}^3$, a difference of one order of magnitude. At $t = 8\,\text{min}$ the difference is a factor of 6, and after $t = 30\,\text{min}$ the difference decreases to a factor of 3. In the other way round, the water exchange of $Q = 90\,\text{mm}^3$ is reached at $t = 30\,\text{min}$ for $A_{\text{cont}} = 231.2\,\text{mm}^2$ and after $t = 300\,\text{min}$ for $A_{\text{cont}} = 8.3\,\text{mm}^2$. The

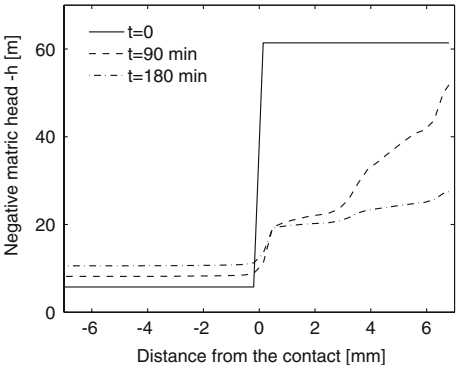

Fig. 11 Evolution of the calculated matric head h across a large aggregate (negative values of the x-axis) and three small aggregates (positive values of the x-axis). The hydraulic gradient in the large initially wet aggregate is very small. The gradient has a peak close to the contacts ($d \approx 0$), and then extends in the region of the small and initially dry aggregates

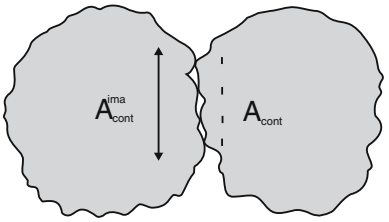

Fig. 12 Contact area between aggregates: under unsaturated conditions the flow cross section A_{cont} is by far narrower than the contact area determined by image analysis $A_{\mathrm{cont}}^{\mathrm{ima}}$. This is primarily due to the presence of air-filled voids within the contact region

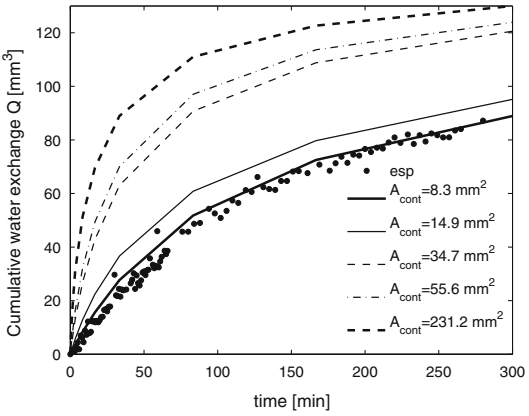

Fig. 13 Sensitivity analysis of A_{cont}. The function $Q(t)$ is calculated for different A_{cont} while keeping $K_{\mathrm{agg}}^{\mathrm{sat}} = 1.0 \times 10^{-7}\,\mathrm{m\,s^{-1}}$ constant

large difference in $Q(t)$ when we increase A_{cont} from 14.9 mm^2 to 34.7 mm^2 is due the formation of new connections between the aggregates.

The discretization of the imaging resolution of three-dimensional domain deserves some comments. In order to describe the flow impedance of the contacts, the effective contact area must be reduced to a minimal size of two to three voxels (Fig. 5). The voxel size of the neutron tomogram (0.125 mm) was apparently small enough to describe the narrow contacts, but we are at the limits of description. With larger voxel sizes the explicit representation of the contacts would have been impossible.

5 Summary and conclusions

We studied the water exchange between wet and dry aggregates packed in a 3 mm thick slab forming a quasi two-dimensional bedding. We used the technique of neutron radiography to monitor the water exchange. By evaluating the attenuation of the neutron beam, we quantified the water content redistribution. The water content remained quite uniform within the aggregates and dropped abruptly at the contacts. This indicates that the contacts have a high flow impedance compared to the aggregate interior.

At equilibrium, we performed a neutron tomography of the sample. Computed tomography algorithms yielded the three-dimensional arrangement of the aggregates. Subsequently, using image analysis we calculated the aggregate volume and the area of the contacts between the wet and the dry aggregates. The contact area determined by image analysis is very likely overestimated because it is of the same order as the spatial resolution the neutron radiographs.

The water flow was simulated in the three-dimensional geometry of the aggregate packing by numerically solving the Richards equation. The aggregates were considered as homogeneous media linked with narrow contacts having the same properties as the aggregates themselves. The aggregate conductivity and the area of the contacts were adjusted in order to match the modelled and observed water flow. In order to vary the contact area, the contact voxels of the tomogram were stepwise removed by the morphological operation called erosion. The optimized contact area turned out to very narrow, in the average 0.015 mm^2 per contact. The narrowness of the contacts is primarily due to air-filled voids within the contact region).

Acknowledgements The authors express their gratitude to Hanspeter Läser (Institute for Terrestrial Ecology, ETH-Zürich) for his precious help and the construction of the experimental setup. Special thanks go to one reviewer for his suggestions and comments that improved the content of this paper and contributed substantially to make it better understandable. We acknowledge the funding of this collaboration effort by these institutions: ETH-Zürich, PSI Villigen, ETH-Lausanne.

References

Barenblatt, G.I., Zheltov, I.P., Kochina, I.N.: Basic concepts in the theory of seepage of homogeneous liquids in fissured rocks. J. Appl. Math. Mech. **24**, 1286–1303 (1960)

Bastian, P.: Numerical computation of multiphase flows in porous media. Abilitation thesis, Christian-Albrechts University, Kiel (1999)

Bayer, A., Vogel, H.-J., Ippisch, O., Roth, K.: Do effective properties for unsaturated weakly heterogeneous media exist? An experimental study. Hydrol. Earth Syst. Sci. **9(5)**, 517–522 (2005)

Braess, D.: Towards algebraic multigrid for elliptic problems of second order. Computing **55**, 379–393 (1995)

Gerke, H.H., Köhne, J.M.: 'Estimating hydraulic properties of soil aggregate skins from sorptivity and water retention. Soil Sci. Soc. Am. J. **66**, 26–36 (2002)

Hassanein, R., Lehmann, E., Vontobel, P.: Methods of scattering corrections for quantitative neutron radiography. Nuclear Instrum Methods Phys Res A **37**, 1093–1106 (2005)

Ippisch, O., Vogel, H.-J., Bastian, P.: Validity limits for the van Genuchten–Mualem model and implications for parameter estimation and numerical simulation. Adv. Water Res., (in press) doi : 10.1016/j.advwatres.2005.12.011 (2006)

Jarvis, N.J.: Macropore and preferential flow. The Encyclopaedia of Agrochemicals, vol. 3, pp. 1005–1013. Wiley and Sons, Inc (2002)

Kaestner, A., Lehmann, P., Carminati, A., Flühler, H.: Analyzing the fabric of soil aggregates. Proc. 2nd Italy-Canada workshop on 3D digital imaging and modeling - Applications of: heritage, industry, medicine and land. Padova, Italy (2005)

Lehmann, P., Kaestner, A., Wyss, P., Carminati, A., H. Flühler: The structure of soil aggregates. PSI Scientific Report 2004 **7**, 99 (2005)
McKenzie, B.M., Dexter, A.R.: Methods for studying the permeability of individual soil aggregates. J. Agric. Eng. Res. **65**, 23–28 (1996)
Mualem, Y.A.: A new model for predicting the hydraulic conductivity of unsaturated porous media. Water Resour. Res. **12**, 513–522 (1976)
Or, D. Wetting-induced soil structural changes: the theory of liquid phase sintering. Water Resour. Res. **32**, 3041–3049 (1996)
Or, D., Ghezzehei, T.A.: Modelling post-tillage soil structural dynamics: a review. Soil Tillage Res. **64**, 41–59 (2002)
Otsu, N.: A threshold selection method from gray-level histograms. IEEE Trans. Syst., Man., Cyber. **9**, 62–66 (1979)
Park, E.-J., Smucker, A.J.M.: Saturated hydraulic conductivity and porosity within macroaggregates modified by tillage. Soil Sci. Soc. Am. J. **69**, 38–45 (2005)
Philip, J.R.: The theory of infiltration: 1. The infiltration equation and its solution. Soil Sci. **83**, 345–357 (1957)
Pleinert, H., Lehmann, E.: Determination of hydrogenous distributions by neutron trasmission analysis. Physica B **234**, 1030–1032 (1997)
Richard, F., Lüscher, P.: hysikalische Eigenschaften von Böden der Schweiz., vol. 3. Swiss Fed. Inst. Forest Res., Birmensdorf (1983)
Schulin, R., Flühler, H., Mansell, R.S., Selim, H.M.: Miscible displacement of ions in aggregated soils. Geoderma **38**, 311–322 (1986)
Soille, P.: Morphological Image Analysis: Principles and Applications, Springer, pp. 267–292 (2003)
Thoma, S.G., Gallegos, D.P., Smith, D.M.: Impact of fracture coatings on fracture/matrix flow interactions in unsaturated porous media. Water Resour. Res. **28**, 1357–1367 (1992)
Vincent, L., Soille, P.: Watersheds in digital spaces: an efficient algorithm based on immersion simulations. IEEE Trans. Pattern Anal. Machine Intell. **13**(6), 583–597 (1991)
Vogel, H.-J., Cousin, I., Ippisch, O., Bastian, P.: The dominant role of structure for solute transport in soil: experimental evidence and modelling of structure and transport in a field experiment. Hydrol. Earth Syst. Sci. **10(4)**, 495–506 (2006)
Vogel, T., van Genuchten, M.T., Cislerova, M.: Effect of the shape of the soil hydraulic functions near saturation on variably-saturated flow predictions. Adv. Water Res. **24**, 133–144 (2001)
Šimůnek, J., Jarvis, N.J., van Genuchten, M.T., Gärdenäs, A.: Review and comparison of models for describing non-equilibrium and preferential flow and transport in the vadose zone. J. Hydrol. **272**, 14–35 (2003)
Zimmerman, R.B., Bodvarsson, G.S.: Absorption of water into porous blocks of various shapes and sizes. Water Resour. Res. **26**, 2797–2806 (1990)